Sipponen, Mika H.; Henn, Alexander; Penttilä, Paavo; Österberg, Monika

Lignin-fatty acid hybrid nanocapsules for scalable thermal energy storage in phase-change materials

Published in:
Chemical Engineering Journal

DOI:
10.1016/j.cej.2020.124711

Published: 01/08/2020

Document Version
Publisher's PDF, also known as Version of record

Chemical Engineering Journal 393 (2020) 124711

Contents lists available at ScienceDirect

Chemical Engineering Journal

journal homepage: www.elsevier.com/locate/cej

Lignin-fatty acid hybrid nanocapsules for scalable thermal energy storage in phase-change materials

Mika H. Sipponen[a,b,*], Alexander Henn[a], Paavo Penttilä[a], Monika Österberg[a,*]

[a] Aalto University, School of Chemical Engineering, Department of Bioproducts and Biosystems, Vuorimiehentie 1, 02150 Espoo, Finland
[b] Department of Materials and Environmental Chemistry, Stockholm University, Svante Arrhenius väg 16 C, 106 91 Stockholm, Sweden

HIGHLIGHTS

- Engineering of hybrid nanocapsules (hyb-NCs) from lignin and fatty acids.
- Size-controlled colloidal synthesis by aqueous co-precipitation.
- Characterization revealed core-shell morphology at the nanoscale.
- Dry and wet hyb-NCs were studied as thermally responsive phase-change materials.

GRAPHICAL ABSTRACT

Fatty acid-lignin hybrid nanocapsules show exceptionally good performance as shape-stabilized phase change materials for thermal energy storage applications.

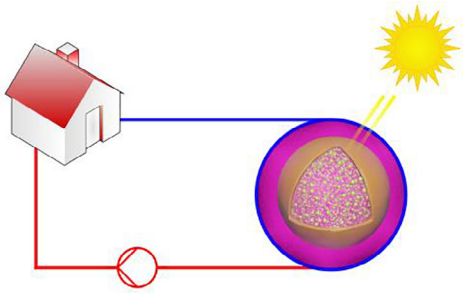

ARTICLE INFO

Keywords:
Colloidal lignin particles
Lignin nanoparticles
Nanocomposite
Thermal energy storage
Hybrid material engineering

ABSTRACT

Development of affordable thermal energy storage (TES) has been hampered by the lack of environmentally benign and scalable phase-change materials (PCM). Here we show size-controlled colloidal synthesis of fatty acid-lignin hybrid nanocapsules and demonstrate their applicability as PCM in dry and wet states. The one-pot fabrication allowed for facile preparation of hybrid capsules with a predictable concentration of tall oil fatty acid, oleic acid, or lauric acid in core-shell particles stabilized by softwood kraft lignin. Phase-change peaks of capsules containing 40 wt% of lauric acid were observed in aqueous dispersion, indicating a possibility to develop colloidal TES systems. In dry form, the hybrid capsules prevented fragmentation of the phase-change peaks during 290 heating-cooling cycles, while in wet state the capsules appeared stable for 25 cycles. The nanoscaled morphology of the capsules was characterized using thermoporometry-differential scanning calorimetry (tp-DSC), transmission electron microscopy (TEM), atomic force microscopy (AFM), dynamic light scattering (DLS), and small angle X-ray scattering (SAXS). Extraction of lauric acid from the capsules allowed for investigation of the intraparticle space previously occupied by the fatty acid. The fatty acid-deficient nanocapsules were found to contain an internal volume that was 19 times as high as that of lignin nanoparticles. Approximately 20 nm thick lignin shells of the capsules were found to be readily accessible to water, permitting heat transfer across the capsules. The possibility to tailor the hybrid capsules by altering the chain length and saturation degree of the fatty acids opens applications that extend beyond the TES systems.

* Corresponding authors at: Department of Materials and Environmental Chemistry, Stockholm University, Svante Arrhenius väg 16 C, 106 91 Stockholm, Sweden (M.H. Sipponen) and Aalto University, School of Chemical Engineering, Department of Bioproducts and Biosystems, Vuorimiehentie 1, 02150 Espoo, Finland (M. Österberg).
E-mail addresses: mika.sipponen@mmk.su.se (M.H. Sipponen), monika.osterberg@aalto.fi (M. Österberg).

https://doi.org/10.1016/j.cej.2020.124711
Received 29 November 2019; Received in revised form 6 February 2020; Accepted 6 March 2020
Available online 08 March 2020

1. Introduction

Mitigation of climate change requires actions to develop clean and energy efficient technologies to reduce greenhouse gas emissions. The residential sector represents 27% of the global energy consumption that is growing especially in the developing countries [1]. It has therefore become pivotal to develop materials and processes for harvesting and storage of thermal energy [2,3]. One of the promising systems is based on phase-change materials (PCMs) that can be used in thermal energy storage applications [3,4]. Typical PCMs rely on the storage and liberation of energy during the solid–liquid transition of fossil hydrocarbons [5–8] and synthetic polymers such as polyethyleneglycol [9], which should be replaced by abundantly available renewable materials.

It is known that for use in large-scale applications, such as for moderating the temperature in buildings [10], a PCM needs to be chemically inert with its surroundings in its molten state, inexpensive, and possess a high heat conductivity and latent heat of fusion [11,12]. Insufficient stability of PCMs is a particular problem requiring new material and engineering solutions. Previously, carbonized materials and porous silica have been used in shape-stabilized PCMs [13,14], while metal, metal oxide, and carbonaceous nanomaterials have been used to improve their heat transfer rates [4,15–17]. Dynamic systems require PCM suspensions that remain colloidally stable while pumping the fluid. Nanoconfinement in core-shell structures is one of the approaches to achieve homogeneous PCM dispersions and to avoid phase separation during the melting stage [18–20]. However, previous literature is lacking simple, low-cost, and scalable colloidal synthesis methods to produce hybrid nanomaterials entirely from renewable biomass resources. Addressing this challenge is important for paving the way for sustainable expansion of PCMs in thermal energy storage applications.

Recent works on encapsulation of organic molecules in lignin nano/micro particles [21,22] and capsules [23–26] triggered our interest in lignin as a component of nanoconfined PCMs. Lignin consists of a group of structurally complex polyphenols with several important functions in green plants [27]. Lignins isolated from pulp and paper production are typified with a polydisperse size distribution that influences their solubility properties [28,29]. Previously, lignin has been used in polymer blends [30] and as a source of carbonaceous support for PCM [31], but lignin-based hybrid materials have not to date been applied as PCM for thermal energy storage applications.

The main objective of this work was to develop a facile and scalable preparation method of lignin-fatty acid capsules and investigate their use as a new type of PCM and related properties for thermal energy storage. We envisioned that such hybrid nanocapsules (hyb-NCs) could be formed by harnessing the emulsion-stabilizing properties of lignin [25,28,32–34] in the self-assembly of fatty acids as a low molecular weight lipophilic substance with phase-changing capability. In order to understand the marked thermal stability of the new PCM capsules, we provide comparative data on the morphology and intraparticle porosity of softwood kraft lignin, lignin nanoparticles (LNPs), and hyb-NCs based on transmission electron microscopy (TEM), atomic force microscopy (AFM), thermoporometry-differential scanning calorimetry (tp-DSC), and small angle X-ray scattering (SAXS) experiments.

2. Materials and methods

2.1. Materials

This work used softwood kraft lignin “BioPiva 100” that was characterized previously by us [35]. Tall oil fatty acid (TOFA) with a tradename “For2” was obtained from Forchem Oyj (Finland) and according to the manufacturer contained 96% fatty acids and an iodine value of 154 [36]. Lauric acid (purity ≥ 98%) was purchased from Sigma-Aldrich, and purified oleic acid (81% Oleic acid, 11% linoleic acid, 3% palmitic acid, 2% stearic acid, and ≤1% palmitoleic acid) and acetone (purity ≥ 99.8%) were purchased from VWR Chemicals. Deionized water was used in all experiments as a source of water.

2.2. Methods

2.2.1. Preparation of hybrid nanocapsules, LNCs and LNPs

Preparation of hybrid nanocapsules (hyb-NCs) was carried out at room temperature in three steps. First, lignin and fatty acid (TOFA, lauric acid, or oleic acid) were dissolved separately in acetone:water 3:1 w/w solvent mixture. Secondly, the solutions were combined in a predefined ratio to obtain a lignin-lipid solution mixture. Thirdly, hyb-NCs were formed by addition of deionized water into a gently stirred solution mixture, and acetone was removed by rotary evaporation under reduced pressure at 40 °C. We note that extensive stirring, rapid addition of water, or the reverse order of mixing the solution with water gave rise to heterogeneous dispersions. For DSC measurements in aqueous dispersion state, hyb-NCs were prepared as above by co-precipitation of lauric acid and lignin (10 g L^{-1} of both components in acetone:water 3:1 w/w) by slow water addition to obtain 100 mL of the dispersion. After evaporation of acetone, the dispersion was concentrated by centrifugation (30 min at 10500 rpm), collecting the sediment phase.

Lignin nanocapsules (LNCs) were obtained by dialysis of lauric acid-lignin hyb-NCs against deionized water that was periodically changed during 24 h. LNPs were prepared similarly as hyb-NCs, but in the absence of fatty acids and with vigorous stirring during the precipitation step. For DSC and FTIR measurements in dry state, the dispersions were freeze dried after the removal of acetone.

2.3. Microscopic analysis

For AFM imaging particle dispersions were diluted to 0.1 wt% and spin-coated onto dry, freshly polyethylenimine-coated mica plates at 2000 rpm for 2 min and dried overnight under ambient conditions. The samples were imaged in tapping mode in ambient air using a Multimode 8 AFM with a Nanoscope V controller (Bruker, Santa Barbara, CA, USA) using NCHV-A probes (Bruker). For TEM imaging of LNPs, hyb-NCs and LNCs the samples were deposited on carbon-coated (3 nm thickness) copper square mesh grids and dried under ambient conditions. TEM images of LNPs, LNCs, and hyb-NCs were acquired in bright-field mode on a FEI Tecnai 12 operating at 120 kV. Polarized light microscopy was performed at 20 to 80 °C on Zeiss Axio Scope A1 polarized light microscope equipped with a heating stage and Zeiss 5x and 20x Zeiss objectives.

2.4. Particle size and zeta potential measurements

Particle size and surface charge were analyzed using a Malvern Zetasizer Nano-ZS90 instrument (UK). A dip cell was used for the determination of Zeta potential of the dispersions (at native pH of 3.6) based on the measured electrophoretic mobility data using the Smoluchowski model.

2.5. Thermoporometry-DSC analysis

Pore size distribution of the particles were analyzed using a differential scanning calorimeter (DSC) 6000 (Perkin Elmer, U.S) following the thermoporometry-DSC (tp-DSC) method adapted from Driemeier et al. [37] as described earlier [38]. Briefly, tp-DSC measurements of aqueous dispersions were carried out at 0.2%, 1.0% and 5.0% (LNPs) or 0.2% (LNCs and SKL) weight percentage concentrations in 50 μL aluminum pans. The pore volume V_{pi} was calculated according to Eq. (1) based on the subtraction in the melting point of water confined within pores of the particles when melted stepwise:

$$V_{pi} = \frac{\Delta H_i - C_{p,\,\mathrm{ice}} \times \Delta T_i}{q_i \times \rho_{i,\,\mathrm{water}}} \quad (1)$$

where, ΔH_i is the measured enthalpy change, $C_{p,\,ice}$ is the specific heat of ice, ΔT_i is the programmed temperature change, q_i is the specific enthalpy of the melted ice, and $\rho_{i,\,water}$ is the density of water at the temperature T_i.

2.6. Thermal characterization

DSC was used to record melting and solidification enthalpies of TOFA, lauric acid, oleic acid, hyb-NCs, and LNCs. The samples were analyzed in dry and wet dispersions states on a DSC 6000 (Perkin Elmer) instrument at a heating rate of 5 °C min^{-1} under 20 mL min^{-1} nitrogen flow.

2.7. Evaluation of thermal stability by FTIR analysis

Lauric acid and freeze-dried LNPs and hyb-NCs were analyzed using a Spectrum Two FT-IR spectrometer (PerkinElmer, U.S.A) with 40 scans per measurement and a resolution of 1 cm^{-1}. To evaluate lauric acid leakage from the hyb-NCs, the particles were analyzed as described above and then heated for one hour in 60 °C in four cycles. The particles were kept in a 4 mL glass vial during the process, and samples of ca. 5–10 mg were carefully taken from the top. Absorbance intensities from aromatic skeletal vibrations (1513 cm^{-1} and 1597 cm^{-1}) and C–H in plane deformation (1140 cm^{-1}) were calculated relative to the intensity of the C=O stretch at 1698 cm^{-1} to assess stability of lauric acid in hyb-NCs. The signals were assigned according to previous literature [39].

2.8. SAXS experiments

Dispersions of LNPs and LNCs at concentrations of 10 g L^{-1} and 1 g L^{-1} were subjected to SAXS measurements at Diamond Light Source on beamline B21, a dedicated beamline for solution state SAXS measurements equipped with a high-throughput, small-volume liquid-handling robot (BioSAXS, Arinax). The measurements were done using an X-ray wavelength of 0.947 Å and with a distance of 2.7 m between the sample and the Eiger detector (Dectris). Absolute intensity was calibrated against a water standard and the q axis using a silver behenate reference. For each liquid sample, a volume of 50 µL was injected into a glass capillary and 20 data frames with 2-s exposure time were collected at 20 °C and 60 °C as the sample was flowed through the X-ray beam path to minimise the effects of radiation damage. The sample cell was washed thoroughly between measurements. Initial data reduction was performed automatically using standard protocols (DAWN, http://dawnsci.org/) and the subsequent data inspection, frame averaging, background correction and rebinning were done using the SAXSutilities software (http://www.saxsutilities.eu/). The SAXS intensities were fitted with the function

$$I(q) = \frac{A}{V}\int f(x)F^2(q,x)dx + B \quad (2)$$

where A and B are coefficients, V is the particle volume, $f(x)$ is the distribution function of variable x , and $F(q,x)$ the scattering amplitude of a particle.

In fitting the intensities of the LNPs, the scattering amplitude of homogeneous spheres was used:

$$F(q) = 3V(\Delta\rho)\left[\frac{\sin(qR) - qR\cos(qR)}{(qR)^3}\right] \quad (3)$$

Here, R is the sphere radius, $V = 4\pi R^3/3$ is the sphere volume and $\Delta\rho$ the scattering length density difference between the two phases. Values of 13.0 × 10^{10} cm^{-2} and 9.5 × 10^{10} cm^{-2} were used for lignin and water, respectively [40]. The radius R was assumed to have a log-normal distribution described by parameters μ and σ:

$$f(R) \propto \frac{1}{R\sigma}e^{\left[-\frac{1}{2}\left(\frac{\ln(R)-\mu}{\sigma}\right)^2\right]} \quad (4)$$

where σ corresponds to the polydispersity of R and the mean radius $R_{mean} = e^{(\mu+\sigma^2/2)}$.

The SAXS intensities of the LNCs were fitted using the scattering amplitude of core-shell spheres:

$$F(q) = \frac{3}{V_s}\left[V_c(\rho_c - \rho_s)\frac{\sin(qR_c) - qR_c\cos(qR_c)}{(qR_c)^3} + V_s(\rho_s - \rho_{solv})\frac{\sin(qR_s) - qR_s\cos(qR_s)}{(qR_s)^3}\right] \quad (5)$$

where R_c and $R_s = R_c + t$ are the radii of the core and shell (thickness t), respectively, and V_c and V_s are the corresponding volumes. The approximate scattering length density of lignin was used for the shell (ρ_s = 13.0 × 10^{10} cm^{-2}) and that of water for the solvent (ρ_{solv} = 9.5 × 10^{10} cm^{-2}), whereas the scattering length density of the core (ρ_c) was allowed to vary between these two values. For the core radius R_c, a log-normal distribution with fixed mean (200 nm) and polydispersity (0.5) values was used. A Gaussian distribution around a mean value t_{mean} with fixed polydispersity $\sigma_t/t_{\mathrm{mean}}$ = 0.15 was assumed for the shell thickness:

$$f(t) \propto e^{\left[-\frac{1}{2}\left(\frac{t-t_{mean}}{\sigma_t}\right)^2\right]} \quad (6)$$

All fitting was done using the SasView 4.2 software (http://www.sasview.org/) and weighting the data points by individual error bars.

3. Results and discussion

3.1. Fabrication of fatty acid-lignin hybrid nanocapsules

The first goal of this work was to develop a simple and scalable method to prepare lignin-fatty acid hybrid capsules. It is well known that fatty acids can be used to produce lignin esters with altered solubility and thermal properties [41–44]. Our hypothesis was that co-precipitation of fatty acids and lignin would suffice to produce self-assembled nanostructures. We expected that fatty acids would precipitate prior to, or simultaneously with, the least water-soluble lignin molecules, causing hierarchical structure formation. Spontaneous formation of hyb-NCs occurred upon addition of water as a non-solvent into the solution mixture of softwood kraft lignin and fatty acids in aqueous acetone (Fig. 1). At this step, it was important to avoid vortex formation while increasing the water content of the solvent mixture to 80 wt%. A proposed mechanism for the formation of hyb-NCs involves three steps: (1) Precipitation and self-assembly of fatty acids into NPs; (2) Stabilization of fatty acid NPs by lignin molecules; (3) Enclosure of lignin-stabilized fatty acid NPs in capsules with relatively thick lignin shells.

Several pure and mixed fatty acids can be used in the fabrication of hyb-NCs. We focused on demonstrating material properties of hyb-NCs with a series of fatty acids with different degrees of saturation and melting points: TOFA, oleic acid (containing 11% of linoleic acid and trace amounts of other fatty acids), and pure lauric acid. TOFA was selected because likewise to the lignin that we employed, it is isolated industrially from softwood during the kraft pulping process [45]. Furthermore, TOFA is in liquid state at room temperature due to its unsaturated fatty acid composition. Unlike the heterogeneous particles obtained from TOFA without lignin (Fig. S1), homogeneous dispersions of TOFA-lignin hyb-NCs could be formed at various weight ratios of the components (Fig. S2). The particle diameter increased from 122 nm to 190 nm and the polydispersity from 0.07 to 0.16 as the theoretical

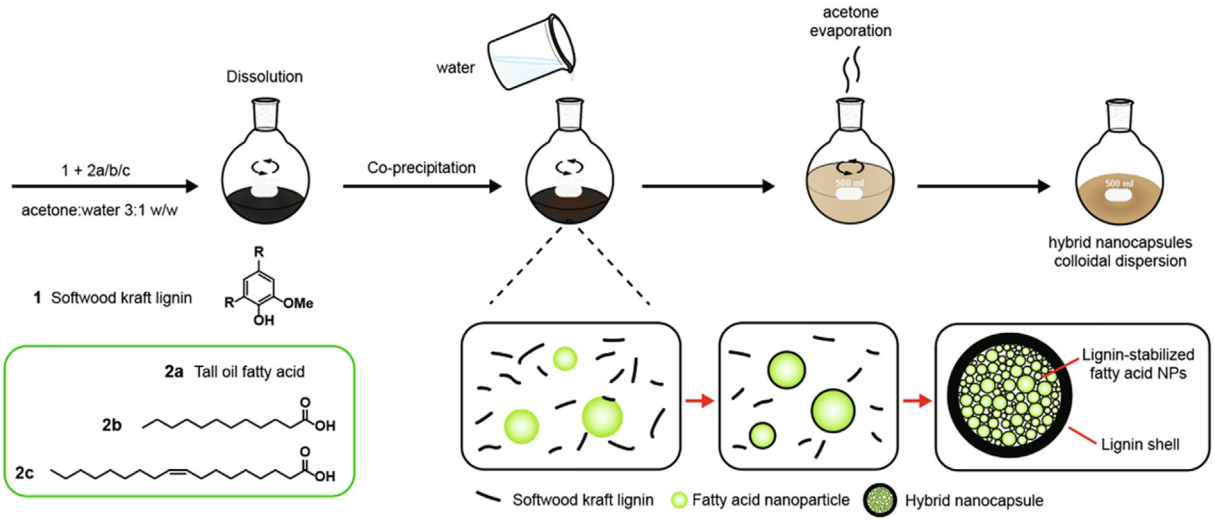

Fig. 1. One-pot method and a proposed formation mechanism of hybrid lignin-fatty acid nanocapsules. 2b, lauric acid; 2c, oleic acid. Note: not drawn to scale.

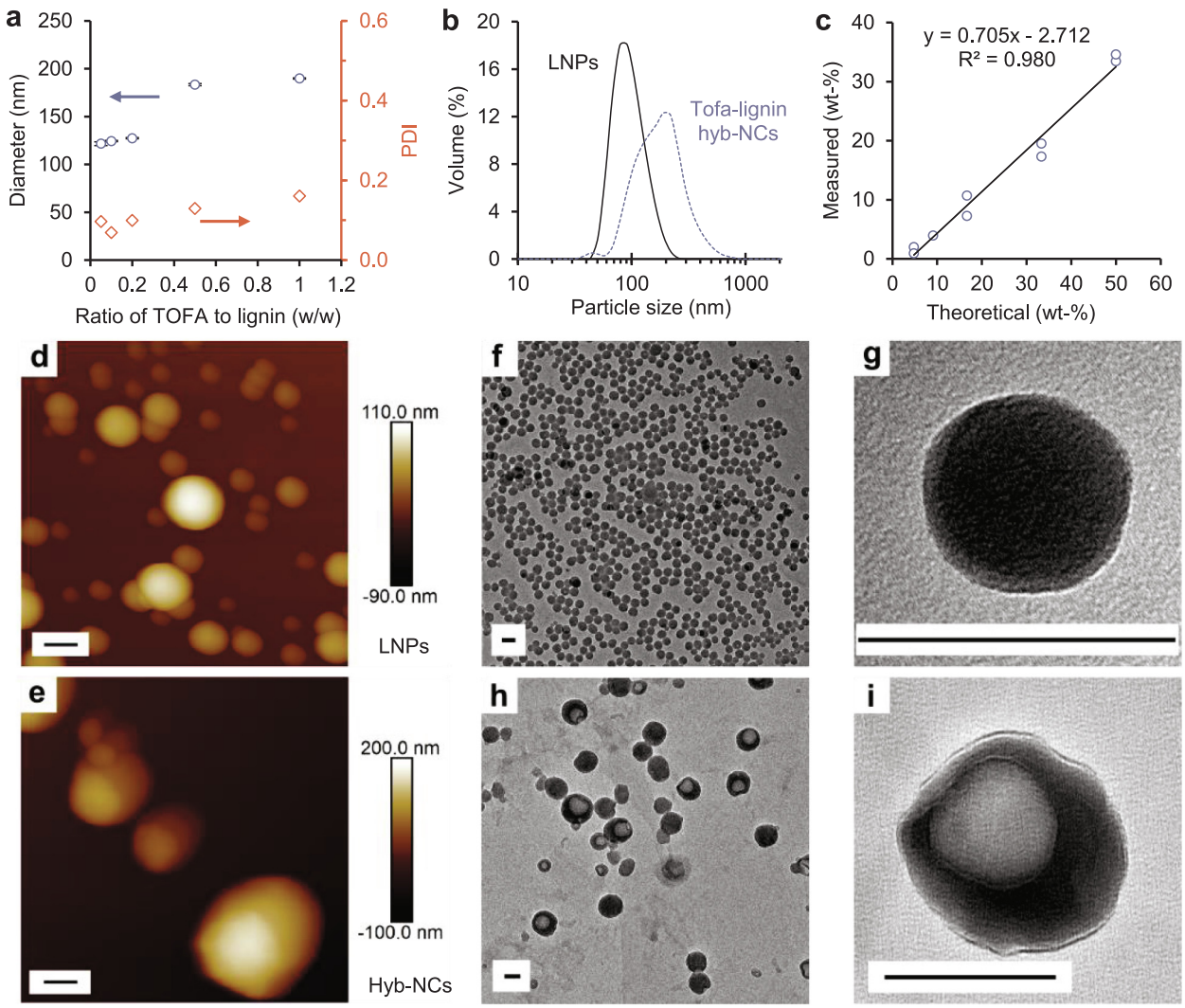

Fig. 2. Colloidal properties and appearance of TOFA-lignin hybrid nanocapsules. (a) Particle diameter and polydispersity of TOFA-lignin hyb-NCs as a function of the theoretical TOFA to lignin weight ratio. (b) Size distribution curves of LNPs and TOFA-lignin hyb-NCs (1:1 w/w) from DLS measurements. (c) Comparison of theoretical and measured TOFA contents of hyb-NCs. AFM height images of (d) LNPs and (e) TOFA-lignin (1:1 w/w) hyb-NCs. TEM images of (f–g) LNPs, (h-i) TOFA-lignin (1:5 w/w) hyb-NCs. Scale bars (black) = 100 nm.

weight ratio of TOFA to lignin was raised from 0.05 to 1 (Fig. 2a). Consequently, hyb-NCs showed a broader size distribution than LNPs formed in the absence of TOFA (Fig. 2b).

TEM and AFM images revealed that compared to the compact particle morphology of LNPs (Fig. 2d, f, g), TOFA-lignin hyb-NCs exhibited core-shell morphologies (Fig. 2e, h, i) and some ruptured capsules that allowed for estimation of the shell thickness of 18 ± 5 nm (Fig. S1). We note than TOFA alone did not form particles with core shell morphologies, but instead particles with broad size distribution when precipitated in the absence of lignin (Fig. S1). Based on the latent heat of fusion of TOFA (68.5 J/g, as measured by DSC), the encapsulation efficiency of TOFA was 71% regardless of the theoretical TOFA content of the hybrid NPs (Fig. 2c). This linearity suggests that the concentration of TOFA in the hybrid capsules could be increased beyond the highest theoretical weight ratios presented herein. It is also evident that the internal volume of the hybrid capsules that we describe here is larger than those of the hollow lignin nanocapsules reported earlier [46,47].

These hyb-NCs with liquid fatty acid cores can be useful for encapsulation of lipophilic substances for drug delivery [48]. Moreover, the small size and colloidal nature of hyb-NCs facilitates their dispersion in composite matrices. We prepared composite films by dispersing 25 wt% of TOFA-lignin hyb-NCs (1:1 w/w) in aqueous PVA solution and letting the mixture to evaporate to dryness under ambient conditions (Fig. S3). Since their shells are made of hydrophilic lignin, hyb-NCs provide a means to homogeneously disperse TOFA or other hydrophobic compounds in water-miscible polymer matrices without phase separation.

Hyb-NCs were spontaneously formed also when lauric acid or oleic acid were used as a pure fatty acid component. The higher melting point of oleic acid gave more durable capsules compared to the ones with TOFA at the similar 1:1 wt ratio to lignin. No ruptured capsules were observed despite the larger size of the capsules (Z-average particle diameter 257 nm) compared to those with TOFA-lignin (190 nm). TEM images captured at higher magnifications revealed mobile fatty acid NPs inside a single hyb-NC (Fig. 3). It is not evident if this packing pattern is prevalent in all hyb-NCs, but this observation nonetheless supports our hypothesis of their formation mechanism (Fig. 1). Furthermore, an emulsion-type core fraction would explain why no phase separation of TOFA or oleic acid was observed from hyb-NC dispersions stored at room temperature.

It is plausible to assume that the production process of hyb-NCs is scalable since the lignin raw material is available in large scale from the pulp and paper industry [49,50] and the co-precipitation is simple and does not require additional surfactants or chemical synthesis. For comparison, sodium dodecyl sulfate has been used as surfactant to emulsify palmitic acid [51] and stearic acid [52] in water for interfacial synthesis of silica shells. The resulting nanocapsules had a shell thickness of 10–30 nm, i.e. in the similar range as the shells of TOFA-lignin hyb-NCs prepared by the facile co-precipitation method in the present work.

3.2. Hybrid nanocapsules as phase-change material

Compared to the triglyceride oils previously used in lignin microcapsules [23,25], fatty acids have a higher heat of fusion and are more broadly available from non-food lipid resources and waste oils. To evaluate suitability of the hybrid capsules for thermal energy storage, it was imperative to determine the exact concentration of the thermally responsive fatty acid component in the hybrid material. We used experimentally determined latent heat of fusion of TOFA (68.5 J/g), oleic acid (100.0 J/g), and lauric acid (176.6 J/g) to calculate the weight percentage and encapsulation efficiency (EE) of the fatty acids in hyb-NCs. This series shows that the latent heat increases as the degree of fatty acid saturation increases. The measured latent heat of fusion of lauric acid-lignin hyb-NCs (1:1 w/w) was 71.4 J/g, which translates to an encapsulation efficiency of 80.8% and a loading concentration of 40.4 wt%. These values are higher than the respective ones obtained with TOFA (EE = 70.5%, 35.3 wt%) and oleic acid (72.9%, 36.4 wt%). Lauric acid and oleic acid were selected to further demonstrate thermal

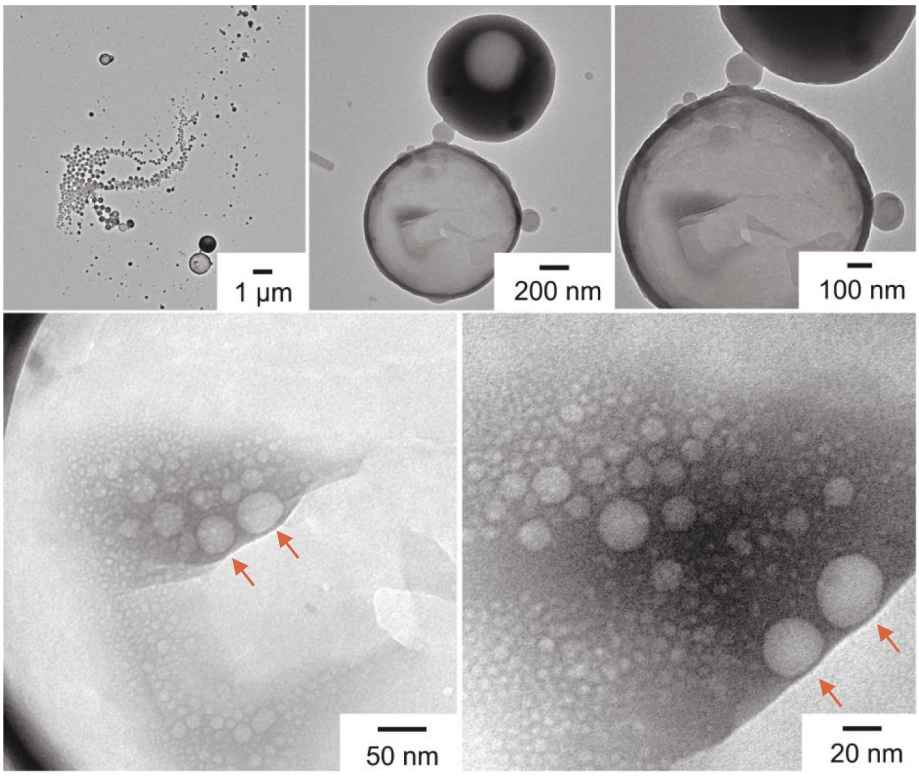

Fig. 3. TEM images of oleic acid-lignin hyb-NCs (1:1 w/w).

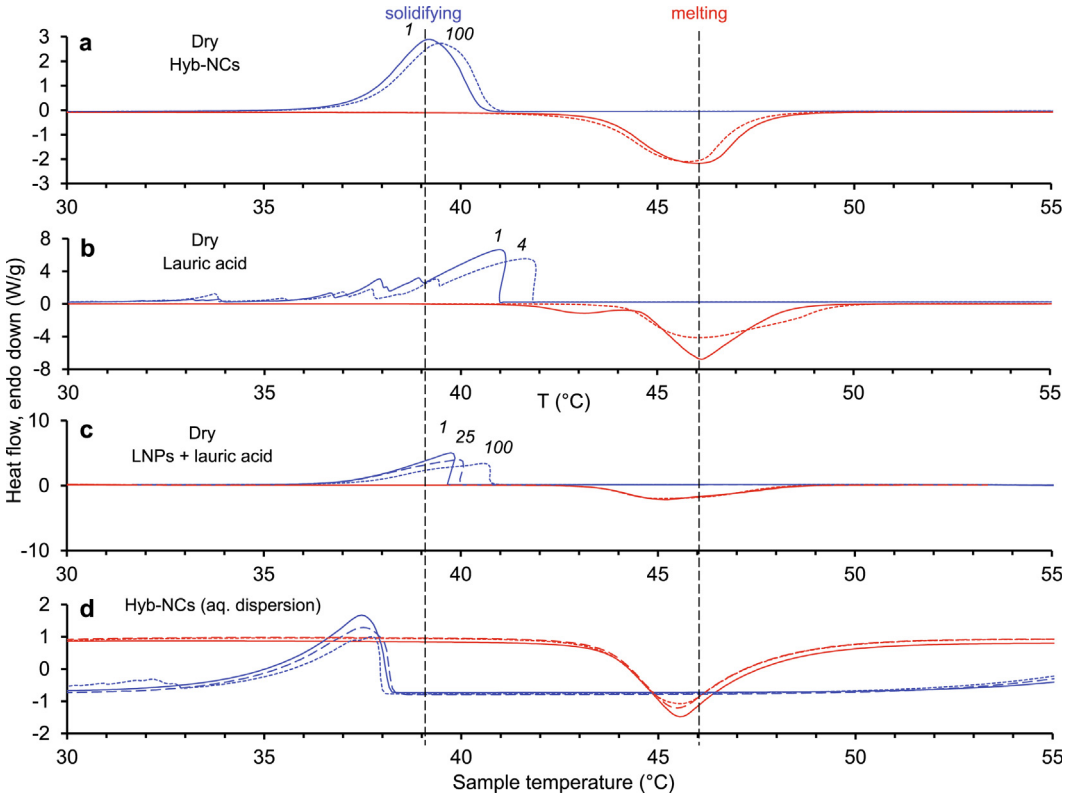

Fig. 4. DSC thermograms showing heating-cooling cycles of (a) Dry lauric acid-lignin hyb-NCs (1:1 w/w) after one (continuous line) and 100 (dashed line) cycles. (b) Pure lauric acid with a total of four thermal cycles. (c) Mixture of lauric acid and LNPs (48:52 w/w) with one, 25, and 100 cycles. (d) DSC thermograms recorded from 14 wt% aqueous dispersion of lauric acid-lignin hyb-NCs. Heat flow is shown relative to the dry substance. Heating and cooling scans from one (continuous lines), 10 (– – –) and 25 (···) cycles are shown.

stability and evaluate the properties of the hybrid capsules as PCM. TOFA was excluded since it showed two broad melting peaks at −45…−2 °C and is as such impractical for the PCM application (Fig. S4). Hyb-NCs with 1:1 wt ratio of lauric acid to lignin were freeze-dried for DSC analysis.

Hyb-NCs containing lauric acid exhibited excellent thermal stability in dry state. The first 100 cycles are shown in Fig. 4a, displaying only a minor shift in the exothermic solidifying peak of lauric acid from 39.2 °C to 39.5 °C. Neither the solidifying peak nor the melting peak at 46.0 °C to 45.8 °C shifted thereafter as monitored up to 290 cycles (Fig. S5). This stability of the hybrid material was notably better than that of pure lauric acid (Fig. 4b). In the absence of lignin, the melting endotherm of pure lauric acid broadened and the solidifying peak at 41.0 °C fragmented towards higher and lower temperature regions already after four thermal cycles. In contrast, the solidifying peak of lauric acid in the hyb-NCs was more symmetrical compared to that of pure lauric acid. Unlike previously studied palmitic acid in silica-shelled capsules [51] the PCM did not show any supercooling. A similar stabilizing trend was observed with the hyb-NCs containing oleic acid (Fig. S6).

We suggest that the augmented stability is a direct consequence of the nanoconfinement of lauric acid inside the lignin-based core-shell nanocapsules. The literature is lacking direct lignin-based benchmarks, and while polysaccharides have been used to modulate properties of poly(urea–formaldehyde) capsules [53], there are not many examples of renewable polymers as sole structural components in PCMs altogether. Instead, many groups have reported nanoencapsulated and nanoconfined PCM systems using non-renewable materials. For instance, palmitic acid has been stabilized in PCMs by encapsulation in graphene oxide (GO) nanoplatelets [17] and oleylamine-functionalized reduced graphene oxide [54]. The former PCM showed stable phase change peaks without supercooling after 2500 thermal cycles [17], while the latter material was used for absorption of simulated sunlight for thermal energy storage [54]. Although sunlight to heat conversion was not in the scope of the current work, we note that melamine foam doped with reduced GO and subsequently impregnated with paraffin wax was recently suggested as a form-stable PCM that combines shape memory property and light-to-thermal energy storage capability [55].

Another study on carbonaceous supports for PCM used acid-oxidized multi-walled carbon nanotubes, which could stabilize 20 wt% of beeswax in a type of form-stable nanocomposite [56]. Zhao et al. studied carbonized vegetable specimens as well as carbonized wood as matrices for vacuum impregnation of PEG [16,57]. A weight fraction of 67% of PEG was achieved in carbonized wood that additionally improved thermal conductivity compared to pristine PEG. The shape-stabilized material showed only minor shifts in the phase change peaks after 200 thermal cycles. Compared to the aforementioned approaches requiring hazardous acid treatment of relatively expensive carbon nanotubes or two-stage carbonization and vacuum impregnation steps, the production method described in the present work is simpler and more environmentally friendly as it does not require the use of corrosive acids or fossil chemicals. For comparison we note that the latent heat of octadecylamine stabilized in a graphene sponge was 93.8% after 200 thermal cycles compared to the initial value of the fatty amine [58]. In the present work, the lignin-lauric acid hybrid material showed higher enthalpy retention values of 99.7% and 98.1% for the solidification and melting enthalpies after 290 cycles compared to the initial enthalpies.

To deduce how lauric acid was stabilized in the hyb-NCs, we compared the thermal behaviour of lauric acid that was merely mixed with dry LNPs with the behavior of hyb-NCs. It turned out that the melting peak of lauric acid in the mixture was stable, but the solidifying peak shifted gradually towards a higher temperature region (Fig. 4c). We postulate that when physically mixed together, LNPs absorbed molten

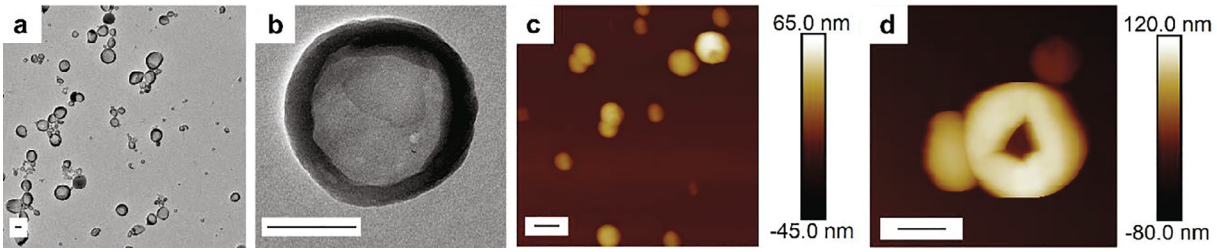

Fig. 5. Representative microscopic images of LNCs. (a-b) TEM micrographs and (c-d) AFM height images of LNCs prepared from lauric acid-lignin 1:1 w/w hyb-NCs. Scale bars (black) = 100 nm.

lauric acid and this infusion in the lignin matrix promoted crystallization of lauric acid by size reduction and nucleation effects [59]. These contrastive results indicate a molecular level association of the fatty acids with lignin in the hybrid materials. During cooling, lignin confines solidification of the fatty acids within the capsules, resisting broadening and separation of the phase transition peaks [10], which offers beneficial stability and prolonged use of the PCM in thermal energy storage applications.

Thermal stability is important also if the hybrid capsules were to be used in practical applications such as wallboards for moderating temperature variation of buildings [60–62]. To assess their thermal stability, hyb-NCs were heated in dry state at 60 °C with measurement of FT-IR spectra at one hour intervals. Compared to the spectrum of the original freeze-dried hyb-NCs, thermally treated hyb-NCs showed a slight drop in the aromatic/carbonyl intensity ratios after one hour at 60 °C, but no changes thereafter (Fig. S7). These results indicate that the hyb-NCs could act as sponges that absorb any leaked lauric acid and prevent phase separation, as also confirmed by the photographs taken from the heated vials containing hyb-NCs. Microscopic investigation revealed softening of freeze-dried lauric acid-lignin hyb-NCs upon heating to 85 °C (Supplementary Video 1 and Fig. S8). Considerably higher temperature than the T_m of lauric acid was needed to cause visible structural changes, which is in accordance with our findings that the fatty acid component was structurally stabilized inside the hyb-NCs. Therefore, hyb-NCs are promising candidates for structurally stabilized PCMs.

In addition to the static thermal energy system, we assessed the hybrid capsules as PCM in aqueous dispersion state. The benefit of such an "active" thermal energy harvesting system [10] is that water that is conventionally used in heat transfer applications can be used to absorb the released latent heat. When measured against deionized water as reference, a concentrated suspension of hyb-NCs (lauric acid to lignin 1:1 w/w) exhibited single endothermic (45.5 °C) and exothermic (37.5 °C) peaks attributed to the melting and solidifying of lauric acid (Fig. 4d). Regardless of the rather low effective concentration of lauric acid in the aqueous dispersion (5.6 wt%), the dry mass-based crystallization enthalpy was similar (71.1 J/g) as found for the dry (71.4 J/g) material. The phase-change peaks were quite stable in the aqueous suspension during 25 consecutive scans. Prolonged thermal cycling shifted the solidifying peak towards a lower temperature region (Fig. S9). It is not evident whether these shifts resulted from phase separation or not, but from a practical point of view it would be beneficial to maintain the dispersion in a continuous flow.

Mofijur et al. reviewed PCMs for a plethora of different applications such solar energy storage, solar water heating, and heat exchange systems, as well as latent heat storage in solar-to-power conversion [63]. Pumpable suspension integrated to a thermal collector circuit would be ideal for temperature modulation of buildings in areas with a high day-night variation in the outdoor temperature. Although these demonstrations were out of scope of the present work, the hybrid nanocapsule dispersion that we prepared could be further evaluated in solar water heating systems.

3.3. Morphological analysis of nanocapsules

The previously discussed direct microscopic analyses and thermal tests showed that fatty acids were stabilized in hyb-NCs. We hypothesized that this structural stability resulted from an internal network structure of hyb-NCs. To test this hypothesis, it was necessary to extract the hyb-NCs, and to remove the fatty acid component for comparison of the resulting porous lignin capsules to compact LNPs that were formed in the absence of fatty acids.

Due to its slight water-solubility, we selected to investigate the capsules containing lauric acid. We found that lauric acid could be removed from the capsules by sequential dialysis as confirmed by DSC analyses (Fig. S10). The resulting lignin nanocapsules (LNCs) maintained their original core-shell morphology (Fig. 5) and hydrodynamic diameter (148.4 ± 1.7 nm) compared to those of hyb-NCs (147.1 ± 1.4 nm) (Fig. 6a–d). The fatty acid-deficient LNCs allowed us to study the particle properties and intra-particle volume previously occupied by lauric acid.

LNCs showed a similar ζ-potential (−29.2 ± 1.2 mV) but had a broader size distribution of 30–300 nm compared to −30.4 ± 0.9 mV and 30–200 nm of LNPs, respectively (Fig. 6a). The diameter of the LNCs could be controlled from 92 nm to 140 nm by altering the weight fraction of lauric acid from 0.05 to 1 in the precursor hyb-NCs (Fig. 6b). Another means to control the size of hyb-NCs or LNCs is to alter the dispersion concentration while keeping the fatty acid to lignin ratio constant. At a weight ratio of 1:1 (lauric acid to lignin), the particle diameter increased linearly from 83 nm to 529 nm when the dispersion concentration of their hyb-NC precursors increased from 0.2 wt% to 2.5 wt% (Fig. 6c). Previous works have reported both a linear correlation [21] and nonlinearity [64,65] between particle size and dispersion concentration of LNPs, but direct comparison to the present work is difficult since different solvents and concentration ranges were used. It was interesting to observe that although their external dimensions did not change, TEM analysis showed that the removal of lauric acid had a clear impact on the internal morphology of hyb-NCs. The shell thickness correlated better with the size of the capsules after the extraction than before (Fig. 6d), indicating that some of the fatty acids associated with the capsule shells were removed in the dialysis step.

The maximum internal volume fraction of the nanocapsules was 62% and the median 34% among 74 capsules subjected to manual measurements of TEM images. Single component lignin nanocapsules have been previously obtained from unpurified kraft lignin [46,66]. Among two-component systems, interfacial polycondensation of toluene diisocyanate (TDI) and ethylene diamine (EDA) gave capsules with a solid paraffin core and a diameter of 498 nm [67]. Another example of prior research is the interfacial polymerization of lignin-polyurethane "nanocontainers" that had a mean diameter of 311 to 390 nm in water and a mean shell thickness of 10–20 nm [68]. These literature values would lead to higher internal volume fractions than obtained in the present work, but our capsules appeared more durable in AFM and TEM images.

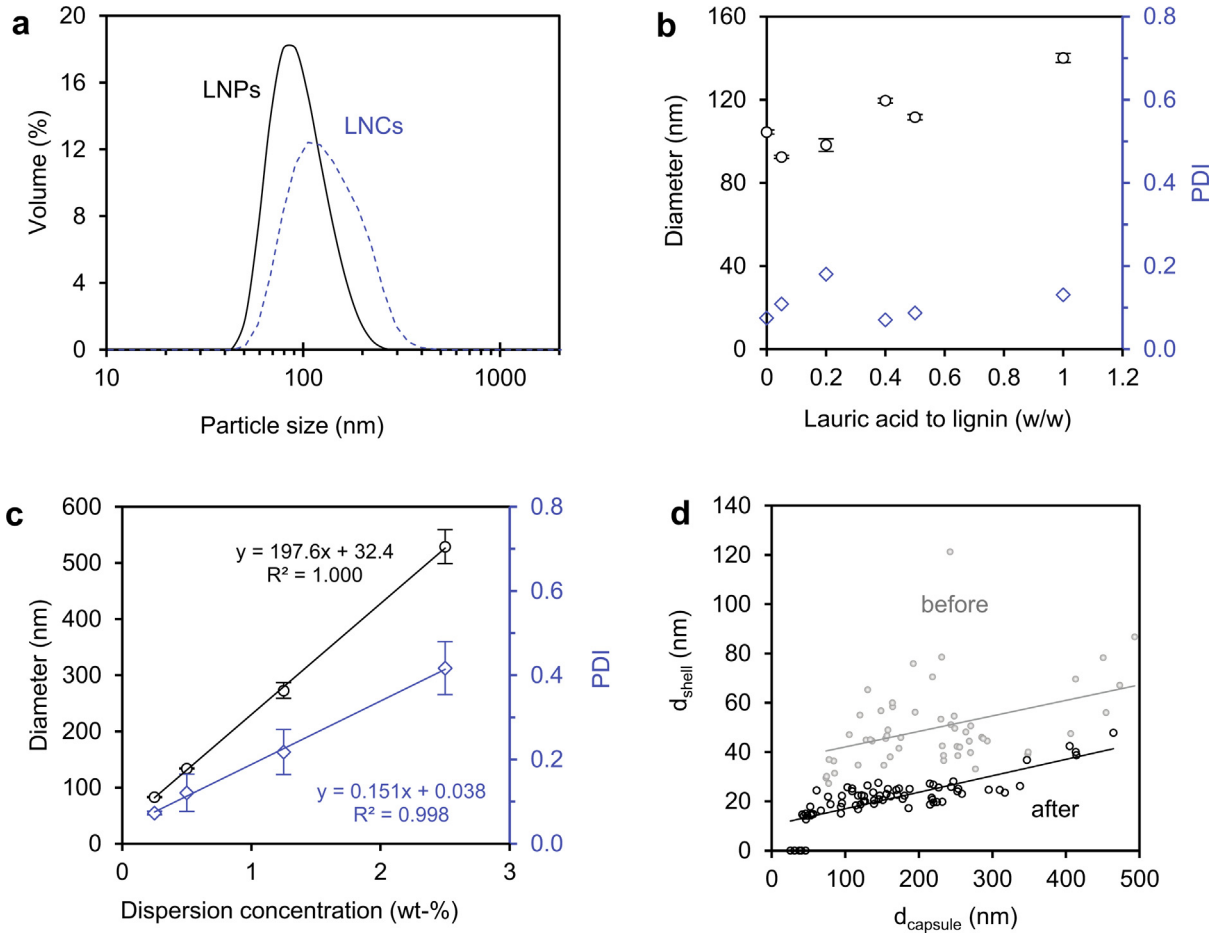

Fig. 6. Colloidal properties of lignin nanoparticles, fatty acid-deficient nanocapsules and hyb-NCs. (a) DLS-based size distribution curves of LNPs and LNCs (1:1 lauric acid-lignin hyb-NCs as precursor). (b) DLS-based particle diameter and polydispersity of LNCs prepared at varying lauric acid to lignin ratio. (c) DLS-based concentration dependence of diameter and polydispersity index (PDI) of hyb-NCs. (d) Shell thickness as a function of capsule diameter before and after extraction of fatty acids from hyb-NCs.

3.3.1. Intraparticle porosity analysis

Understanding the intraparticle porosity is important to assess heat conduction in the PCM application. The pore size distributions of fatty acid-deficient LNCs were calculated from tp-DSC data (see Fig. S11 for example of thermograms) and compared to the values of LNPs and the starting lignin material (SKL in aqueous suspension). Preliminary results for LNPs showed that the qualitative and quantitative pore volume-pore diameter distributions are dependent on the suspension concentration of the sample. We measured LNPs at 0.2 wt%, 1 wt% and 5 wt% concentrations (Fig. S12) and concluded that the most dilute dispersion should be the most ideal for these measurements to avoid aggregation that might overestimate the apparent pore volumes. All measurements were thus made at 0.2 wt% concentration.

In stark contrast to LNPs and SKL, LNCs exhibited a markedly different porosity profile (Fig. 7a). The pore volume distributions of LNCs showed highest pore volumes between pore diameters of 100 nm and 200 nm, while LNPs and SKL showed maxima at an approximate pore diameter of 5.5 nm. These results are explained by the presence of a hollow core-shell structure and lend explanation for the fact that the cumulative pore volume of LNCs reached 89.9 mL g^{-1} compared to 4.7 mL g^{-1} and 6.6 mL g^{-1} with LNPs and SKL, respectively (Fig. 7b). Although DLS and TEM data showed that the number of large capsules was low, their relative contribution to the pore volume is more significant. Equally interesting is the fact that LNPs and SKL showed almost similar pore size distributions (Fig. 7a). The main difference was observed in the region with 30–400 nm pore sizes, with clearly lower pore volumes in LNPs than in SKL. This finding is reasonable on the basis of the size distribution of LNPs that showed only a minor amount of particles with diameter > 200 nm (Fig. 2b), whereas aggregation and acid-precipitation of kraft lignin from alkaline solution is known to give rise to interpenetrating networks with pores in the dimensions found here [69–71].

Before this study, very little was known about the nanoscaled morphology of LNPs unlike that of conformation and association of lignins in solution [72–78]. In tetrahydrofuran solution, softwood kraft lignin molecules have shown a radius of gyration of 1.67 nm and ellipsoidal morphology with a maximum dimension of 6.5 nm [72]. In solid state, softwood kraft lignin has exhibited surface fractals at the length scale of 3.5 nm and above [73]. Although a direct line cannot be drawn between the molecular dimensions in different solvent systems, it appears that aggregation and precipitation of lignins form materials with intrinsically high porosity in solid state. Lignin-based carbonaceous materials have shown total pore volumes of 0.91 [79] and 2.7 [80] mL g^{-1} based on nitrogen adsorption isotherms, but loss of the initial porosity may occur in the course of melting of lignin during the carbonization process.

There are only a few reports on pore size distribution of non-carbonized lignins in the submicrometer scale. Driemeier et al. used tp-DSC to observe the contribution of lignin to the nanoscale porosity of native and pretreated lignocelluloses [81]. They found that removal of lignin increased pores with diameter between 10 nm and 200 nm, and that 4 nm pores appeared to be specific to lignin. This is in accordance with our findings with isolated lignins, as 5–6 nm pore sizes were the most prevalent ones in LNPs and SKL (Fig. 7a). On the other hand,

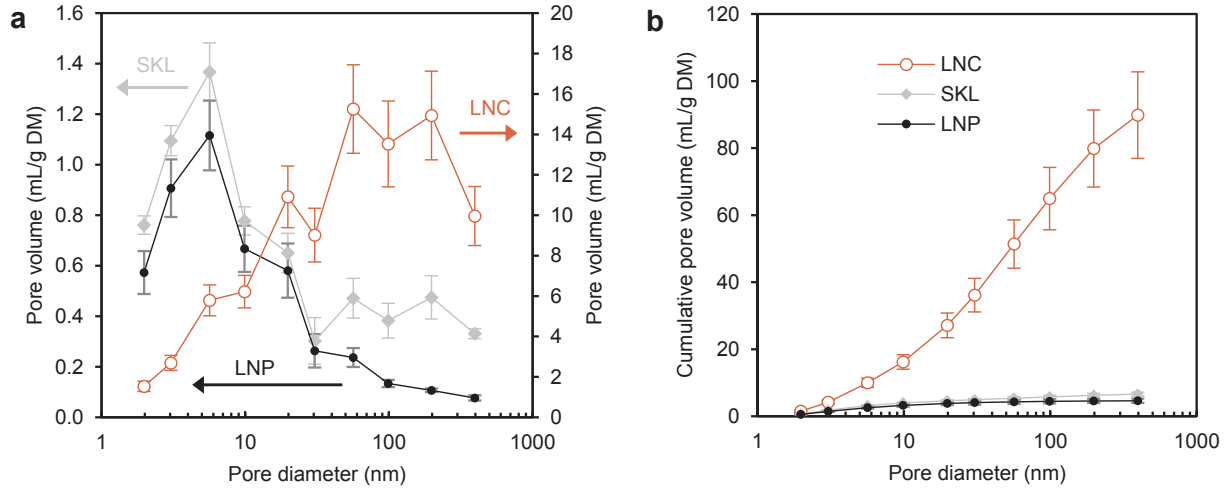

Fig. 7. (a) Pore size distributions and (b) Cumulative pore sizes of LNPs, SKL and LNCs. Data points show mean values ± one standard deviation (n = 4).

Dizhbite et al. reported based on mercury intrusion porosimetry data that hydrolysis lignins from bioethanol production contained pores with radii between 3.3 nm and 36 μm, and 500–5000 nm was the region with the most abundant pore radii [82]. These particle sizes are markedly higher than the ones found here for SKL and LNPs. All these different results likely depend on the differences in the lignin raw material, and the different lignin sources and methods of tracing pores. In mercury intrusion porosimetry, liquid mercury is forced into the porous material under pressure, which measures interpenetrating pore networks as single pores, while in tp-DSC such pore systems would confine crystallization and melting of ice in a series of individual pores that give a different pore size distribution.

3.3.2. Comparative SAXS investigation of LNPs and LNCs

The contrastive porosity profiles of LNPs and LNCs sparked our interest in undertaking a more detailed SAXS analysis. TEM images of the LNCs used in these SAXS experiments are shown in Fig. S13. The measurements were carried out at two concentrations and temperatures to compare structural stability of the materials. Examples of SAXS intensities from LNPs and LNCs at 20 °C and 60 °C are shown in Fig. 8 and the data from all samples are included in Fig. S14. All of the curves showed a region of power-law decay with the intensity approximately proportional to q^{-4} (dashed straight lines in Fig. 8 for comparison), which indicates smooth surfaces at least in the scale of some tens of nanometers [83].

At low q values (below $q = 10^{-2}$ Å^{-1}), the intensities of the LNPs approached a constant value, which suggests that the typical particle size in these samples was below 100 nm (sphere diameter around 80 nm based on Guinier law) [83]. This value is between those measured by image analysis of dry particles in TEM images (sphere diameter 47 nm, Fig. S15) and the hydrodynamic diameter obtained from the DLS data (102 nm, Fig. 6a). In order to include the particle shape and a distribution of sizes in the SAXS analysis, an expression for solid spheres with log-normal size distribution (Eqs. (2), (3), (4)) was used to fit the intensities from the LNPs (Fig. 8a). The fits yielded a mean diameter of 34 nm and polydispersity close to 0.40 at 20 °C (Table S1). The relatively high value of polydispersity could be at least partly explained by a deviation from the assumed spherical shape of the particles. A slightly smaller diameter (29 nm) and larger polydispersity (0.43) were obtained for the single sample measured at 60 °C, which might indicate smaller size of the particles at higher temperatures. The SAXS results of the LNPs are consistent with the q^{-4} power law behavior down to

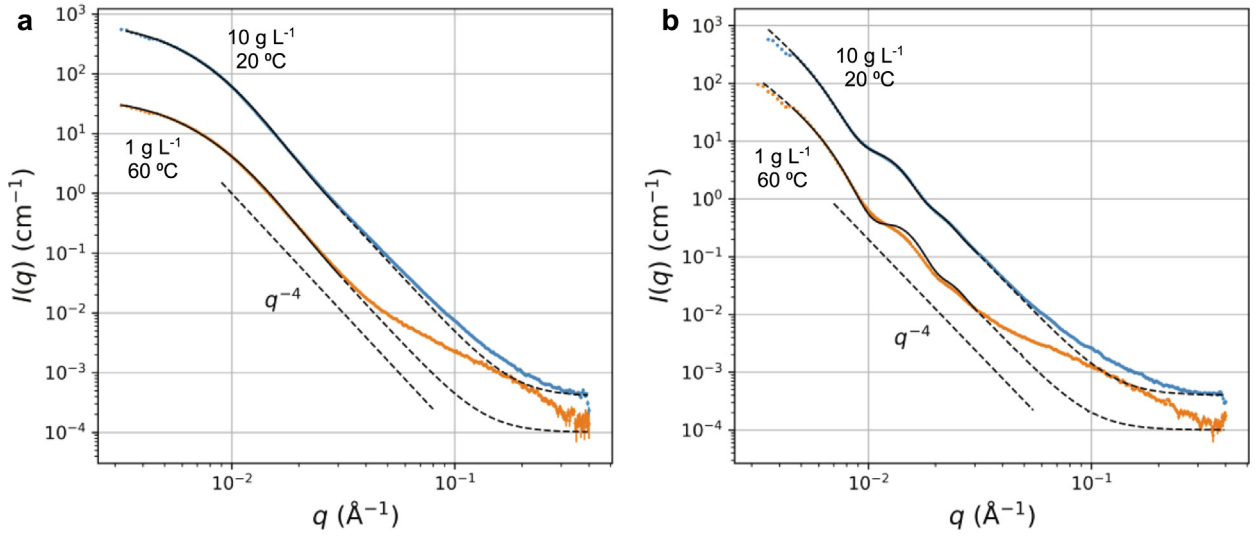

Fig. 8. Comparative SAXS data (blue and orange dots) with fits indicated by solid lines in the fitting range and with dashed line outside of it: (a) LNPs fitted with a model for solid spheres, (b) LNCs fitted with a model for spherical shells. For both graphs, top curve represent a dispersion concentration of 10 g L^{-1} measured at 20 °C, whereas the lower curve stands for a concentrate of 1 g L^{-1} measured at 60 °C. (For interpretation of the references to colour in this figure legend, the reader is referred to the web version of this article.)

q = 0.007 Å^{-1} reported previously for aqueous LNP dispersions prepared from tetrahydrofuran solution of lignin, and interpreted to arise from compact large particles with smooth surfaces [72]. Unlike in their case, the q-range of our data allowed the determination of the outer dimensions of the particles.

Due to the larger dimensions of the LNCs (Fig. S13), the low-q plateau for these particles was outside of the accessible q range, which made it impossible to determine their exact outer dimensions from the current SAXS data. However, the intensity at low-q and mid-q exhibited a modulation around the q^{-4} power law (Fig. 8b), which was assigned to a spherical shell with higher electron density as compared to the inner core and the surrounding solvent [81,84]. The SAXS intensities from the LNCs were therefore fitted with a model for core-shell spheres (Eqs. (2), (5), (6)), where the electron density of the core was limited to values between the assumed lignin shell and the aqueous solvent. With the diameter of the core fixed to 400 nm (based on the value of 421 nm found by DLS) and a large log-normal polydispersity (0.5), the fits yielded a shell thickness of around 66 nm at 20 °C and about 59 nm at 60 °C (Table S2). We note that the LNCs analyzed here were larger than those presented in Fig. 6a–c because they were concentrated by centrifugation that enriched larger capsules in the sample. Based on the fitting results, the electron density of the core lies approximately halfway between those of the shell and the aqueous solution, indicating that the particles were not completely hollow. This observation supports the presence of internal skeletal lignin network that stabilized nanoemulsion droplets in hyb-NCs before the dialysis step that was used to remove lauric acid. Such internal nanodroplet morphology was observed in the case of oleic acid-lignin hyb-NCs (Fig. 3).

At the higher end of the accessible q range, corresponding roughly to real-space distances below 20 nm, all samples deviated from the spherical particle fits and the deviation was larger in the heated samples (Fig. 8 and Fig. S14). This additional contribution at high q values could originate from lignin molecules either in solution or as part of the spherical structures. The increase in this contribution with temperature would be in line with an increasing solubility of low molecular weight lignin fragments at higher temperatures [85,86].

4. Conclusions

In this work, we described a scalable process for the fabrication of hybrid nanocapsules consisting of softwood kraft lignin and fatty acids as renewable building blocks. The hybrid nanocapsules exhibited encouraging properties as stable nanoconfined phase-change materials. Because of their water-accessible shells, the hybrid nanocapsules overcome the poor thermal conductivity of lignin and function well as phase-change material both in dry state and in aqueous dispersion. We further showed that it is possible to extract the hybrid capsules to obtain highly porous capsules containing only lignin. The new insight gained from the SAXS analysis and porosity measurements improves our understanding of the formation mechanism and packing patterns of various lignin morphologies from the same parent lignin. Hybrid nanocapsules are recommended for further development of thermally responsive and composite materials, while porous lignin nanocapsules could be explored as catalyst supports and gas separation materials. Further work could also assess lignin-based hybrid capsules for light-to-thermal energy conversion and storage.

Declaration of Competing Interest

The authors declare that they have no known competing financial interests or personal relationships that could have appeared to influence the work reported in this paper.

Acknowledgements

We acknowledge Diamond Light Source for time on Beamline B21 under Proposal SW24748-1. Dr. Claire Pizzey from Diamond Light Source is thanked for conducting the SAXS measurements. MHS and PP acknowledge funding from the Academy of Finland [grant numbers 296547 and 315768, respectively]. We are also grateful for the support by the FinnCERES Materials Bioeconomy Ecosystem.

Appendix A. Supplementary data

Supplementary data to this article can be found online at https://doi.org/10.1016/j.cej.2020.124711.

References

[1] P. Nejat, F. Jomehzadeh, M.M. Taheri, M. Gohari, M.Z. Muhd, A global review of energy consumption, CO_2 emissions and policy in the residential sector (with an overview of the top ten CO_2 emitting countries), Renew. Sustain. Energy Rev. 43 (2015) 843–862, https://doi.org/10.1016/j.rser.2014.11.066.
[2] G. Zhang, P. Zhao, X. Zhang, K. Han, T. Zhao, Y. Zhang, C.K. Jeong, S. Jiang, S. Zhang, Q. Wang, Flexible three-dimensional interconnected piezoelectric ceramic foam based composites for highly efficient concurrent mechanical and thermal energy harvesting, Energy Environ. Sci. 11 (2018) 2046–2056, https://doi.org/10.1039/c8ee00595h.
[3] A.L. Cottrill, A.T. Liu, Y. Kunai, V.B. Koman, A. Kaplan, S.G. Mahajan, P. Liu, A.R. Toland, M.S. Strano, Ultra-high thermal effusivity materials for resonant ambient thermal energy harvesting, Nat. Commun. 9 (2018) 1–11, https://doi.org/10.1038/s41467-018-03029-x Article number: 664.
[4] H. Ji, D.P. Sellan, M.T. Pettes, X. Kong, J. Ji, L. Shi, R.S. Ruoff, Enhanced thermal conductivity of phase change materials with ultrathin-graphite foams for thermal energy storage, Energy Environ. Sci. 7 (2014) 1185–1192, https://doi.org/10.1039/c3ee42573h.
[5] G. Fang, H. Li, F. Yang, X. Liu, S. Wu, Preparation and characterization of nano-encapsulated n-tetradecane as phase change material for thermal energy storage, Chem. Eng. J. 153 (2009) 217–221, https://doi.org/10.1016/j.cej.2009.06.019.
[6] X. Tang, W. Li, H. Shi, X. Wang, J. Wang, X. Zhang, Fabrication, characterization, and supercooling suppression of nanoencapsulated n-octadecane with methyl methacrylate-octadecyl methacrylate copolymer shell, Colloid Polym. Sci. 291 (2013) 1705–1712, https://doi.org/10.1007/s00396-013-2905-1.
[7] P. Felix De Castro, D.G. Shchukin, New polyurethane/docosane microcapsules as phase-change materials for thermal energy storage, Chem. Eur. J. 21 (2015) 11174–11179, https://doi.org/10.1002/chem.201500666.
[8] C. Shen, X. Li, G. Yang, Y. Wang, L. Zhao, Z. Mao, B. Wang, X. Feng, X. Sui, Shape-stabilized hydrated salt/paraffin composite phase change materials for advanced thermal energy storage and management, Chem. Eng. J. 385 (2020) 123958, , https://doi.org/10.1016/j.cej.2019.123958.
[9] S.B. Sentürk, D. Kahraman, C. Alkan, I. Gökce, Biodegradable PEG/cellulose, PEG/agarose and PEG/chitosan blends as shape stabilized phase change materials for latent heat energy storage, Carbohydr. Polym. 84 (2011) 141–144, https://doi.org/10.1016/j.carbpol.2010.11.015.
[10] G.J. Suppes, M.J. Goff, S. Lopes, Latent heat characteristics of fatty acid derivatives pursuant phase change material applications, Chem. Eng. Sci. 58 (2003) 1751–1763, https://doi.org/10.1016/S0009-2509(03)00006-X.
[11] P.J. da Cunha, P. Eames, Thermal energy storage for low and medium temperature applications using phase change materials – a review, Appl. Energy 177 (2016) 227–238, https://doi.org/10.1016/j.apenergy.2016.05.097.
[12] M. Kenisarin, K. Mahkamov, Solar energy storage using phase change materials, Renew. Sustain. Energy Rev. 11 (2007) 1913–1965, https://doi.org/10.1016/j.rser.2006.05.005.
[13] Y. Lv, W. Situ, X. Yang, G. Zhang, Z. Wang, A novel nanosilica-enhanced phase change material with anti-leakage and anti-volume-changes properties for battery thermal management, Energy Convers. Manag. 163 (2018) 250–259, https://doi.org/10.1016/j.enconman.2018.02.061.
[14] J. Li, L. He, T. Liu, X. Cao, H. Zhu, Preparation and characterization of PEG/SiO_2 composites as shape-stabilized phase change materials for thermal energy storage, Sol. Energy Mater. Sol. Cells 118 (2013) 48–53, https://doi.org/10.1016/j.solmat.2013.07.017.
[15] J.M. Khodadadi, L. Fan, H. Babaei, Thermal conductivity enhancement of nanostructure-based colloidal suspensions utilized as phase change materials for thermal energy storage: a review, Renew. Sustain. Energy Rev. 24 (2013) 418–444, https://doi.org/10.1016/j.rser.2013.03.031.
[16] Y. Zhao, B. Sun, P. Du, X. Min, Z. Huang, Y. Liu, X. Wu, M. Fang, Hierarchically channel-guided porous wood-derived shape-stabilized thermal regulated materials with enhanced thermal conductivity for thermal energy storage, Mater. Res. Express 6 (2019), https://doi.org/10.1088/2053-1591/ab4700.
[17] M. Mehrali, S.T. Latibari, M. Mehrali, T.M.I. Mahli, H.S.C. Metselaar, M.S. Naghavi, E. Sadeghinezhad, A.R. Akhiani, Preparation and characterization of palmitic acid/graphene nanoplatelets composite with remarkable thermal conductivity as a novel shape-stabilized phase change material, Appl. Therm. Eng. 61 (2013) 633–640, https://doi.org/10.1016/j.applthermaleng.2013.08.035.

[18] W. Aftab, X. Huang, W. We, Z. Liang, A. Mahmood, R. Zou, Nanoconfined phase change materials for thermal energy applications, Energy Environ. Sci. 11 (2018) 1392–1424, https://doi.org/10.1039/C7EE03587J.

[19] G.H. Zhang, S.A.F. Bon, C.Y. Zhao, Synthesis, characterization and thermal properties of novel nanoencapsulated phase change materials for thermal energy storage, Sol. Energy 86 (2012) 1149–1154, https://doi.org/10.1016/j.solener.2012.01.003.

[20] X. Min, M. Fang, Z. Huang, Y. Liu, Y. Huang, R. Wen, T. Qian, X. Wu, Enhanced thermal properties of novel shape-stabilized PEG composite phase change materials with radial mesoporous silica sphere for thermal energy storage, Sci. Rep. 5 (2015) 1–11, https://doi.org/10.1038/srep12964.

[21] M.H. Sipponen, H. Lange, M. Ago, C. Crestini, Understanding lignin aggregation processes. A case study: budesonide entrapment and stimuli controlled release from lignin nanoparticles, ACS Sustain. Chem. Eng. 6 (2018) 9342–9351, https://doi.org/10.1021/acssuschemeng.8b01652.

[22] P. Figueiredo, K. Lintinen, A. Kiriazis, V. Hynninen, Z. Liu, T. Bauleth-Ramos, A. Rahikkala, A. Correia, T. Kohout, B. Sarmento, J. Yli-Kauhaluoma, J. Hirvonen, O. Ikkala, M.A. Kostiainen, H.A. Santos, In vitro evaluation of biodegradable lignin-based nanoparticles for drug delivery and enhanced antiproliferation effect in cancer cells, Biomaterials 121 (2017) 97–108, https://doi.org/10.1016/j.biomaterials.2016.12.034.

[23] M. Tortora, F. Cavalieri, P. Mosesso, F. Ciaffardini, F. Melone, C. Crestini, Ultrasound driven assembly of lignin into microcapsules for storage and delivery of hydrophobic molecules, Biomacromolecules 15 (2014) 1634–1643, https://doi.org/10.1021/bm500015j.

[24] N. Chen, L.A. Dempere, Z. Tong, Synthesis of pH-responsive lignin-based nanocapsules for controlled release of hydrophobic molecules, ACS Sustain. Chem. Eng. 4 (2016) 5204–5211, https://doi.org/10.1021/acssuschemeng.6b01209.

[25] T. Zou, M.H. Sipponen, M. Österberg, Natural shape-retaining microcapsules with shells made of chitosan- coated colloidal lignin particles, Front. Chem. 7 (2019) 370, https://doi.org/10.3389/fchem.2019.00370.

[26] E.D. Bartzoka, H. Lange, K. Thiel, C. Crestini, Coordination complexes and one-step assembly of lignin for versatile nanocapsule engineering, ACS Sustain. Chem. Eng. 4 (2016) 5194–5203, https://doi.org/10.1021/acssuschemeng.6b00904.

[27] G. Henriksson, What are the biological functions of lignin and its complexation with carbohydrates? Nord. Pulp Pap. Res. J. 32 (2017) 527–541, https://doi.org/10.3183/NPPRJ-2017-32-04-p527-541.

[28] M.H. Sipponen, M. Smyth, T. Leskinen, L.-S. Johansson, M. Österberg, All-lignin approach to prepare cationic colloidal lignin particles: stabilization of durable Pickering emulsions, Green Chem. 19 (2017) 5831–5840, https://doi.org/10.1039/C7GC02900D.

[29] A.S. Jääskeläinen, T. Liitiä, A. Mikkelson, T. Tamminen, Aqueous organic solvent fractionation as means to improve lignin homogeneity and purity, Ind. Crops Prod. 103 (2017) 51–58, https://doi.org/10.1016/j.indcrop.2017.03.039.

[30] L. Jianchun, Y. He, Y. Inoue, Study on thermal and mechanical properties of biodegradable blends of poly(ε-caprolactone) and lignin, Polym. J. 33 (2001) 336–343.

[31] M.A. Palazzolo, M.-A. Dourges, A. Magueresse, P. Glouannec, L. Maheo, H. Deleuze, Preparation of lignosulfonate-based carbon foams by pyrolysis and their use in the microencapsulation of a phase change material, ACS Sustain. Chem. & Eng. 6 (2018) 2453–2461, https://doi.org/10.1021/acssuschemeng.7b03900.

[32] T.E. Nypelö, C.A. Carrillo, O.J. Rojas, Lignin supracolloids synthesized from (W/O) microemulsions: use in the interfacial stabilization of Pickering systems and organic carriers for silver metal, Soft Matter 11 (2015) 2046–2054, https://doi.org/10.1039/C4SM02851A.

[33] O.J. Rojas, J. Bullón, F. Ysambertt, A. Forgiarini, D.S. Argyropoulos, J.-L. Salager, Lignins as emulsion stabilizers, in: D.S. Argyropoulos (Ed.), Mater. Chem. Energy from For. Biomass, American Chemical Society, Washington, DC, 2007, pp. 182–199 papers2://publication/uuid/D2207A00-5007-4D6C-BD86-AF9C51D4D921.

[34] M. Ago, S. Huan, M. Borghei, J. Raula, E.I. Kauppinen, O.J. Rojas, High-throughput synthesis of lignin particles (~30 nm to ~2 μm) via aerosol flow reactor: Size fractionation and utilization in pickering emulsions, ACS Appl. Mater. Interfaces 8 (2016) 23302–23310, https://doi.org/10.1021/acsami.6b07900.

[35] M.H. Sipponen, M. Farooq, J. Koivisto, A. Pellis, J. Seitsonen, M. Österberg, Spatially confined lignin nanospheres for biocatalytic ester synthesis in aqueous media, Nat. Commun. 9 (2018), https://doi.org/10.1038/s41467-018-04715-6 Article number: 2300.

[36] Product Datasheet FOR2, (n.d.). https://www.forchem.com/files/637/forchem_datasheet_FOR2_003.pdf (accessed August 3, 2019).

[37] C. Driemeier, F.M. Mendes, M.M. Oliveira, Dynamic vapor sorption and thermoporometry to probe water in celluloses, Cellulose 19 (2012) 1051–1063, https://doi.org/10.1007/s10570-012-9727-z.

[38] V. Pihlajaniemi, M.H. Sipponen, H. Liimatainen, J.A. Sirviö, A. Nyyssölä, S. Laakso, Weighing the factors behind enzymatic hydrolyzability of pretreated lignocellulose, Green Chem. 18 (2016) 1295–1305, https://doi.org/10.1039/C5GC01861G.

[39] O. Faix, Classification of lignins from different botanical origins by FT-IR spectroscopy, Holzforschung 45 (Suppl) (1991) 21–27.

[40] M. Martínez-Sanz, M.J. Gidley, E.P. Gilbert, Application of X-ray and neutron small angle scattering techniques to study the hierarchical structure of plant cell walls: A review, Carbohydr. Polym. 125 (2015) 120–134, https://doi.org/10.1016/j.carbpol.2015.02.010.

[41] K.A.Y. Koivu, H. Sadeghifar, P.A. Nousiainen, D.S. Argyropoulos, J. Sipilä, Effect of fatty acid esterification on the thermal properties of softwood kraft lignin, ACS Sustain. Chem. Eng. 4 (2016) 5238–5247, https://doi.org/10.1021/acssuschemeng.6b01048.

[42] S. Laurichesse, C. Huillet, L. Avérous, Original polyols based on organosolv lignin and fatty acids: new bio-based building blocks for segmented polyurethane synthesis, Green Chem. 16 (2014) 3958–3970, https://doi.org/10.1039/c4gc00596a.

[43] W. Thielemans, R.P. Wool, Lignin esters for use in unsaturated thermosets: lignin modification and solubility modeling, Biomacromolecules 6 (2005) 1895–1905, https://doi.org/10.1021/bm0500345.

[44] H. Setälä, H.-L. Alakomi, A. Paananen, G.R. Szilvay, M. Kellock, M. Lievonen, V. Liljeström, E.-L. Hult, K. Lintinen, M. Österberg, M. Kostiainen, Lignin nanoparticles modified with tall oil fatty acid for cellulose functionalization, Cellulose (2019), https://doi.org/10.1007/s10570-019-02771-9.

[45] K. Vienola, G. Jurgens, J. Vuorenmaa, J. Apajalahti, Tall oil fatty acid inclusion in the diet improves performance and increases ileal density of lactobacilli in broiler chickens, Br. Poult. Sci. 59 (2018) 349–355, https://doi.org/10.1080/00071668.2018.1455965.

[46] H. Li, Y. Deng, B. Liu, Y. Ren, J. Liang, Y. Qian, X. Qiu, C. Li, D. Zheng, Preparation of nanocapsules via the self-assembly of kraft lignin: a totally green process with renewable resources, ACS Sustain. Chem. Eng. 4 (2016) 1946–1953, https://doi.org/10.1021/acssuschemeng.5b01066.

[47] F. Xiong, Y. Han, S. Wang, G. Li, T. Qin, Y. Chen, F. Chu, Preparation and formation mechanism of renewable lignin hollow nanospheres with a single hole by self-assembly, ACS Sustain. Chem. Eng. 5 (2017) 2273–2281, https://doi.org/10.1021/acssuschemeng.6b02585.

[48] M.H. Sipponen, H. Lange, C. Crestini, A. Henn, M. Österberg, Lignin for nano- and microscaled carrier systems: applications, trends and challenges, ChemSusChem 12 (2019) 2039–2054, https://doi.org/10.1002/cssc.201900480.

[49] C. Crestini, H. Lange, M. Sette, D.S. Argyropoulos, On the structure of softwood kraft lignin, Green Chem. 19 (2017) 4104–4121, https://doi.org/10.1039/C7GC01812F.

[50] P. Tomani, The lignoboost process, Cell. Chem. Technol. 44 (2010) 53–58.

[51] S. Tahan Latibari, M. Mehrali, M. Mehrali, T.M. Indra Mahlia, H.S. Cornelis Metselaar, Synthesis, characterization and thermal properties of nanoencapsulated phase change materials via sol-gel method, Energy 61 (2013) 664–672, https://doi.org/10.1016/j.energy.2013.09.012.

[52] S. Zhang, S. Wang, J. Zhang, Y. Jiang, Q. Ji, Z. Zhang, Z. Wang, Increasing phase change latent heat of stearic acid via nanocapsule interface confinement, J. Phys. Chem. C 117 (2013) 23412–23417, https://doi.org/10.1021/jp408478h.

[53] Y. Zhang, D. Baiocco, A.N. Mustapha, X. Zhang, Q. Yu, G. Wellio, Z. Zhang, Y. Li, Hydrocolloids: nova materials assisting encapsulation of volatile phase change materials for cryogenic energy transport and storage, Chem. Eng. J. 382 (2019) 123028, , https://doi.org/10.1016/j.cej.2019.123028.

[54] A.R. Akhiani, M. Mehrali, S. Tahan Latibari, M. Mehrali, T.M.I. Mahlia, E. Sadeghinezhad, H.S.C. Metselaar, One-step preparation of form-stable phase change material through self-assembly of fatty acid and graphene, J. Phys. Chem. C 119 (2015) 22787–22796, https://doi.org/10.1021/acs.jpcc.5b06089.

[55] H. Yan Wu, S. Tai Li, Y. Wen Shao, X. Zheng Jin, X. Dong Qi, J. Hui Yang, Z. Wan Zhou, Y. Wang, Melamine foam/reduced graphene oxide supported form-stable phase change materials with simultaneous shape memory property and light-to-thermal energy storage capability, Chem. Eng. J. 379 (2020) 122373, https://doi.org/10.1016/j.cej.2019.122373.

[56] N. Putra, S. Rawi, M. Amin, E. Kusrini, E.A. Kosasih, T.M. Indra Mahlia, Preparation of beeswax/multi-walled carbon nanotubes as novel shape-stable nanocomposite phase-change material for thermal energy storage, J. Energy Storage 21 (2019) 32–39, https://doi.org/10.1016/j.est.2018.11.007.

[57] Y. Zhao, X. Min, Z. Huang, Y. Liu, X. Wu, M. Fang, Honeycomb-like structured biological porous carbon encapsulating PEG: a shape-stable phase change material with enhanced thermal conductivity for thermal energy storage, Energy Build. 158 (2018) 1049–1062, https://doi.org/10.1016/j.enbuild.2017.10.078.

[58] T. Chen, C. Liu, P. Mu, H. Sun, Z. Zhu, W. Liang, A. Li, Fatty amines/graphene sponge form-stable phase change material composites with exceptionally high loading rates and energy density for thermal energy storage, Chem. Eng. J. 382 (2020), https://doi.org/10.1016/j.cej.2019.122831.

[59] K. Weihua, Y. He, N. Asakawa, Y. Inoue, Effect of lignin particles as a nucleating agent on crystallization of poly (3-hydroxybutyrate), J. Appl. Polym. Sci. 94 (2004) 2466–2474, https://doi.org/10.1002/app.21204.

[60] F. Kuznik, J. Virgone, Experimental assessment of a phase change material for wall building use, Appl. Energy 86 (2009) 2038–2046, https://doi.org/10.1016/j.apenergy.2009.01.004.

[61] F. Kuznik, J. Virgone, J. Noel, Optimization of a phase change material wallboard for building use, Appl. Therm. Eng. 28 (2008) 1291–1298, https://doi.org/10.1016/j.applthermaleng.2007.10.012.

[62] P. Schossig, H.M. Henning, S. Gschwander, T. Haussmann, Micro-encapsulated phase-change materials integrated into construction materials, Sol. Energy Mater. Sol. Cells 89 (2005) 297–306, https://doi.org/10.1016/j.solmat.2005.01.017.

[63] M. Mofijur, T.M.I. Mahlia, A.S. Silitonga, H.C. Ong, M. Silakhori, M.H. Hasan, N. Putra, S.M. Ashrafur Rahman, Phase change materials (PCM) for solar energy usages and storage: an overview, Energies 12 (2019) 1–20, https://doi.org/10.3390/en12163167.

[64] K. Lintinen, Y. Xiao, R.P. Bangalore Ashok, T. Leskinen, E. Sakarinen, M.H. Sipponen, M. Farooq, P. Oinas, M. Österberg, M.A. Kostiainen, Closed cycle production of concentrated and dry redispersible colloidal lignin particles with a three solvent polarity exchange method, Green Chem. 20 (2018) 843–850, https://doi.org/10.1039/C7GC03465B.

[65] M. Lievonen, J.J. Valle-Delgado, M.-L. Mattinen, E.-L. Hult, K. Lintinen, M.A. Kostiainen, A. Paananen, G.R. Szilvay, H. Setälä, M. Österberg, Simple process for lignin nanoparticle preparation, Green Chem. 18 (2016) 1416–1422, https://doi.org/10.1039/C5GC01436K.

[66] B. Waste, H. Li, Y. Deng, J. Liang, Y. Dai, B. Liu, Y. Ren, Direct preparation of

hollow nanospheres with kraft lignin: a facile strategy for effective utilization of biomass waste, BioResources 11 (2016) 3073–3083.
[67] S. Park, Y. Lee, Y.S. Kim, H.M. Lee, J.H. Kim, I.W. Cheong, W.G. Koh, Magnetic nanoparticle-embedded PCM nanocapsules based on paraffin core and polyurea shell, Colloids Surf., A 450 (2014) 46–51, https://doi.org/10.1016/j.colsurfa.2014.03.005.
[68] D. Yiamsawas, G. Baier, E. Thines, K. Landfester, F.R. Wurm, Biodegradable lignin nanocontainers, RSC Adv. 4 (2014) 11661, https://doi.org/10.1039/c3ra47971d.
[69] M.H. Sipponen, O.J. Rojas, V. Pihlajaniemi, K. Lintinen, M. Österberg, Calcium chelation of lignin from pulping spent liquor for water-resistant slow-release urea fertilizer systems, ACS Sustain. Chem. Eng. 5 (2017) 1054–1061, https://doi.org/10.1021/acssuschemeng.6b02348.
[70] M. Norgren, H. Edlund, Lignin: Recent advances and emerging applications, Curr. Opin. Colloid Interface Sci. 19 (2014) 409–416, https://doi.org/10.1016/j.cocis.2014.08.004.
[71] L. Alicia, M. Nevárez, L.B. Casarrubias, Biopolymer-based nanocomposites: effect of lignin acetylation in cellulose triacetate films, Sci. Technol. Adv. Mater. 12 (2011) 045006, , https://doi.org/10.1088/1468-6996/12/4/045006.
[72] S. Salentinig, M. Schubert, Softwood lignin self-assembly for nanomaterial design, Biomacromolecules 18 (2017) 2649–2653, https://doi.org/10.1021/acs.biomac.7b00822.
[73] U. Vainio, N. Maximova, B. Hortling, J. Laine, P. Stenius, L.K. Simola, J. Gravitis, R. Serimaa, Morphology of dry lignins and size and shape of dissolved kraft lignin particles by X-ray scattering, Langmuir 20 (2004) 9736–9744, https://doi.org/10.1021/la048407v.
[74] M. Norgren, H. Edlund, L. Wågberg, Aggregation of lignin derivatives under alkaline conditions. Kinetics and aggregate structure, Langmuir 18 (2002) 2859–2865, https://doi.org/10.1021/la011627d.
[75] S. Sarkanen, S. Sarkanen, D.C. Teller, E. Abramowski, J.L. McCarthy, Lignin. 19. Kraft lignin component conformation and associated complex configuration in aqueous alkaline solution, Macromolecules 15 (1982) 1098–1104, https://doi.org/10.1021/ma00232a027.
[76] W. Zhao, L.-P. Xiao, G. Song, R.-C. Sun, L. He, S. Singh, B.A. Simmons, G. Cheng, From lignin subunits to aggregates: insights into lignin solubilization, Green Chem. 19 (2017) 3272–3281, https://doi.org/10.1039/C7GC00944E.
[77] M. Yang, W. Zhao, S. Singh, B. Simmons, G. Cheng, On the solution structure of kraft lignin in ethylene glycol and its implication for nanoparticle preparation, Nanoscale Adv. 1 (2019) 299–304, https://doi.org/10.1039/c8na00042e.
[78] G. Cheng, M.S. Kent, L. He, P. Varanasi, D. Dibble, R. Arora, K. Deng, K. Hong, Y.B. Melnichenko, B.A. Simmons, S. Singh, Effect of ionic liquid treatment on the structures of lignins in solutions: molecular subunits released from lignin, Langmuir 28 (2012) 11850–11857, https://doi.org/10.1021/la300938b.
[79] S. Hu, Y. Lo Hsieh, Ultrafine microporous and mesoporous activated carbon fibers from alkali lignin, J. Mater. Chem. A 1 (2013) 11279–11288, https://doi.org/10.1039/c3ta12538f.
[80] W. Zhang, M. Zhao, R. Liu, X. Wang, H. Lin, Hierarchical porous carbon derived from lignin for high performance supercapacitor, Colloids Surf., A 484 (2015) 518–527, https://doi.org/10.1016/j.colsurfa.2015.08.030.
[81] C. Driemeier, M.M. Oliveira, A.A.S. Curvelo, Lignin contributions to the nanoscale porosity of raw and treated lignocelluloses as observed by calorimetric thermoporometry, Ind. Crops Prod. 82 (2016) 114–117, https://doi.org/10.1016/j.indcrop.2015.11.084.
[82] T. Dizhbite, A. Kizima, G. Rossinskaya, V. Jurkjane, G. Telysheva, Products of Lignin Modification: Promising Adsorbents of Toxic Substances, Woodhead Publishing Limited, 2010, , https://doi.org/10.1533/9781845693749.3.161.
[83] G. Porod, General theory, in: O. Glatter, O. Kratky (Eds.), Small-Angle X-Ray Scatt. Academic Press, London, 1982, pp. 17–51.
[84] T. Li, A.J. Senesi, B. Lee, Small angle X-ray scattering for nanoparticle research, Chem. Rev. 116 (2016) 11128–11180, https://doi.org/10.1021/acs.chemrev.5b00690.
[85] E.I. Evstigneev, Factors affecting lignin solubility, Russ. J. Appl. Chem. 84 (2011) 1040–1045, https://doi.org/10.1134/S1070427211060243.
[86] J. Qing-Zhu, M. Pei-Sheng, Z. Huan, X. Shu-Qian, W. Qiang, Q. Yan, The effect of temperature on the solubility of benzoic acid derivatives in water, Fluid Phase Equilib. 250 (2006) 165–172, https://doi.org/10.1016/j.fluid.2006.10.014.